A NON-PEER-REVIEWED PREPRINT UPLOADED TO ENGRXIV

Younan-Veletsos retaining wall: The exact solution

Joaquin Garcia-Suarez[1]* | **Domniki Asimaki**[2]*

[1]Graduate Aerospace Laboratories, California Institute of Technology, Pasadena, California, 91125, USA

[2]Mechanical and Civil Engineering, California Institute of Technology, Pasadena, California, 91125, USA

Correspondence
Joaquin Garcia-Suarez, Graduate Aerospace Laboratories, California Institute of Technology, Pasadena, California, 91125, USA
Email: ajgarcia@caltech.edu

Funding information

The assessment of forces exerted on walls by the backfill is a recurrent problem in Geotechnical Engineering, owing to its relevance for both retaining systems and underground structures. In particular, the work by Veletsos and Younan becomes pertinent when considering pressure increments on underground structures triggered by seismic events. These scholars furnished the first satisfactory engineering solution corresponding to a simple configuration, which has become a milestone in the field. This paper presents the exact solution to this reference problem. The solution is given in horizontal wavenumber domain, hence it comes in terms of inverse Fourier transforms, which in turn are verified against finite-element simulations. Specific features of this exact solution that were not captured by prior engineering approximations are highlighted and discussed.

KEYWORDS
Geotechnical Engineering , Retaining Walls , Elastodynamics , Mathematical Modelling , Exact Solution

1 | INTRODUCTION

The study of the forces that soil exerts over retaining structures dates back centuries. A first clear distinction can be made on the basis of the methods that have been employed for these studies:

- Methods based on plastic behavior of soils, foremost, limit-state theory [1], for so-called *yielding* walls, that is, walls that move enough as to elicit plastic response in the soil.

* Equally contributing authors.

- Method formulated on the basis of the theory of Linear Elasticity to describe both soil and structure [2], which presupposes small deformation in both soil and wall. The wall in these cases is termed *unyielding*.

The proper approach for the analysis does depend on the typology of the wall that is to be assessed or designed. Static load scenarios can be designed following the classic methods [3]; on the contrary, when it comes to considerations in the dynamic earthquake setting, the right choice remains unclear to this day.

On one hand, yielding walls require consideration of the soil plastic behavior in the time-domain, and thus researchers have proposed *pseudo-static* methods, that, in spite of intrinsic limitations, deliver satisfactory, even conservative, outcomes for free-standing gravity or cantilever walls (except if resting on stiff rock). On the other hand, approaches based on Linear Elasticity are suitable to ascertain seismic pressures on unyielding walls (as, e.g., restrained basement walls or rigid-enough underground structures), as long as the structure whose walls are being analyzed does not experience other soil-structure interaction (SSI) effects (rocking). The National Earthquake Hazard Reduction Program (NEHRP) recommendations [4] sanction this classification, while also suggest that a wall whose top deflects around 0.2% of its height already triggers plastic behavior in its soil vicinity, ergo the threshold to consider a wall as yielding is in practice fairly narrow.

The influence of soil-structure interaction, the effect of water in the backfill, the role of soil cohesion on the seismic response, as well as other topics, are still subjects of ongoing study.

1.1 | Approaches based on Limit-state Theory

Pertaining to the first group, the forerunner is the classic method devised by Coulomb [3], under the tenets of what nowadays is called limit-state theory [1]. This method was developed to describe the response of yielding walls (sliding or rotating) under the action of its own weight and the weight of the backfill. Its adaptation, for cohesionless soils, to attempt to consider also accelerations due to earthquakes came after the great Kanto earthquake (1923), which devastated a number of retaining walls (in particular, the quay walls of the harbor of Yokohama), and it is referred to as the Mononobe-Okabe (M-O) Method [5].

A number of similar improved schemes were developed later [6, 7], leading to the a state-of-the-art model by Mylonakis and collaborators [8].

All these methods framed the problem in a pseudo-static setting, wherein the earthquake load is idealized as a horizontal acceleration that is considered concurrently with gravity. One can acknowledge the inherent limitations of such approaches:

- They assume that the wall has already deformed outward (away from the soil) so as to generate an active earth pressure, and assume an active soil wedge that extends from the base of the retaining wall to the surface.
- The soil behind the wall behaves as a rigid body, so accelerations are uniform along the interface between wall and soil. Ignoring wave propagation phenomena and their oscillatory nature, these approaches are unable to provide the actual, time-varying distribution of pressures, just an estimate of the resultant force. This issue becomes increasingly apparent as the height of the wall increases.
- Finally, the framework cannot accommodate a-posteriori wall flexibility, even on a local scale: either the wall moves as a rigid body or it remains completely still.

Moreover, there is a lack of consensus both on how to define the earthquake acceleration, and how to consider backfill heterogeneity. In spite of these issues, these methods enjoy wide use to this day and seem to provide satisfactory

design for peak ground acceleration (PGA) as high as 0.4 g [9].

1.2 | Approaches based on Elasticity

When straining of both the soil and wall remains relatively small, Linear Elasticity theory provides a proper framework to describe its evolution. The only completely rigorous solution (from the mathematical standpoint) using this approach was obtained by Wood [10]. He considered a 2D finite stratum of soil on rigid bedrock confined between walls deforming under linear-elastic plane-strain conditions. While this configuration may resemble a different system at first, logic dictates that if the distance between walls increases, the effects of one wall over the other one must fade, leaving the system virtually equivalent to the one-wall configuration insofar the displacements field around the wall are concerned. Hence, the problem may well be dubbed the *singular* Wood's problem.
Nevertheless, his solution's mathematical "decorum" is overshadowed by being unintuitive (the mathematical expressions do not lend themselves to straightforward physical interpretation), in particular when the distance between walls tends to infinity, and also troublesome to evaluate numerically.

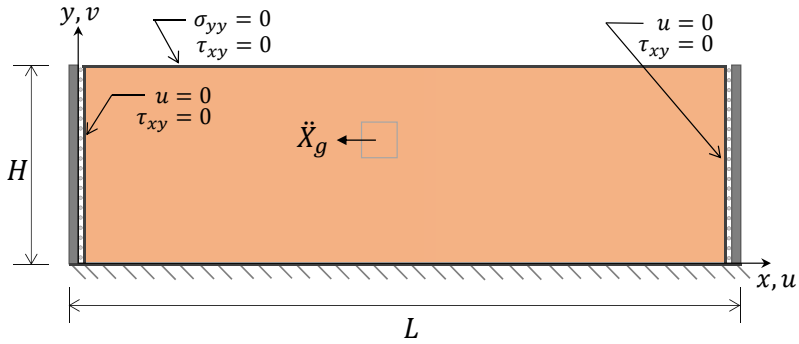

FIGURE 1 System solved by Wood (1973)

Simplified models for one-wall systems have been developed throughout the years in order to circumvent this issue, but every effort of tackling this very problem relied on introducing various forms of simplification.

The first attempt to consider a one-wall system directly trace back to the work by Matsuo and Ohara [11]. They assumed a *confined solution* [12] in which no vertical displacement develops anywhere in the soil domain, not even at regions close to the wall. This solution was shown to be unbounded in the incompressible-material limit (undrained soil conditions).

The classic solutions for the one-wall case are those derived by Veletsos and Younan [13, 14]. In the first, a variation of the confined solution was utilized: instead of neglecting a component of the displacement field, these researchers assumed that no normal vertical stress develops anywhere in the soil ($\sigma_{yy} = 0$ everywhere) in order to simplify and solve the equations of motion, thus retrieving the displacement field over the whole domain. Regrettably, satisfying vertical equilibrium and the boundary condition $\tau_{xy}|_w = 0$ became impossible due to the introduction of this severe simplification.

In the second, [13], a substantial improvement on Scott's model [15] was presented. It was assumed that the soil stratum behaves as an elastically-supported, semi-infinite horizontal viscoelastic bar with distributed mass, and that the horizontal gradient of vertical displacements in the calculation of shear stresses is negligible. A solution was thus derived for the medium impedance, that related the stress field on the wall to the simpler displacement field in the

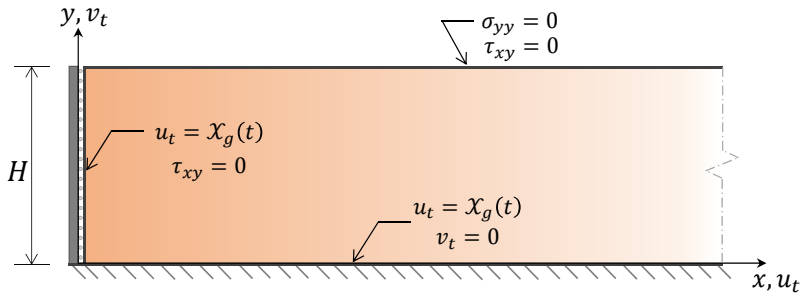

FIGURE 2 System framed in terms of total displacements

far-field (referred as "1D soil column" or "shear beam"). Later [16], their analysis was refined to consider different wall typologies, yet the foregoing simplifications were kept. Nevertheless, this work became the first one in attempting to include the effect on wall flexibility on the magnitude and distribution of pressures.

State-of-the-art models, as those proposed by Kloukinas and collaborators [17], later used in the already-mentioned "kinematic framework" proposed by Brandenberg and colleagues [18], have been directly influenced by the Veletsos-Younan landmark work [13], and have inherited the same pivotal assumption to simplify the equations of motion: normal vertical stresses are forced to be zero everywhere, $\sigma_{yy} = 0$.
A more detailed summary of these and other previous studies can be found in a recent paper by [19].

In this paper, we provide the exact solution of the Younan-Veletsos problem, computed with no physical or mathematical simplifications. The solution procedure is inspired by to those recurrently furnished on the basis of the Elastic Waveguide Theory [20], and does not resort to any unconventional mathematics. Results are given in the form of algebraic expressions in the horizontal wave-number domain, and compared against results of finite-element simulations in the spatial domain. We also discuss features of the exact solution that we have identified were absent from simplified solutions, and ponder in what cases these features become relevant.

2 | DERIVATION OF THE EXACT SOLUTION IN HORIZONTAL WAVE-NUMBER DOMAIN

The system shown in Figure 2 comprises of a rigid wall connected to a rigid base (bedrock) and restraining a layer of soil. No specific boundary conditions, other than rigidity, were used for the wall in Veletsos and Younan's original work, as the simplifying constraint they introduced, $\sigma_{yy} = 0$, precluded these consideration anyway. Following Wood [10], we shall consider that the wall is *smooth*, i.e., frictionless, and thus no shear stress develops at the soil-wall interface.

2.1 | Presentation: total displacements

Consider an semi-infinite soil layer, resting on rigid bedrock and bounded to the left by a rigid (moves with the bedrock base) and smooth (thus no shear stress develops at the interface) wall.

The excitation of the system is an imposed time-varying displacement at the base $\mathcal{X}_g(t)$. Assuming that the soil behaves as a homogeneous, density ρ, isotropic linear-elastic solid (characterized by Lamé parameters μ, shear modulus, and λ), undergoing small deformations, the equations that govern the dynamic response of the material are the so-called Cauchy-Navier equations [12]:

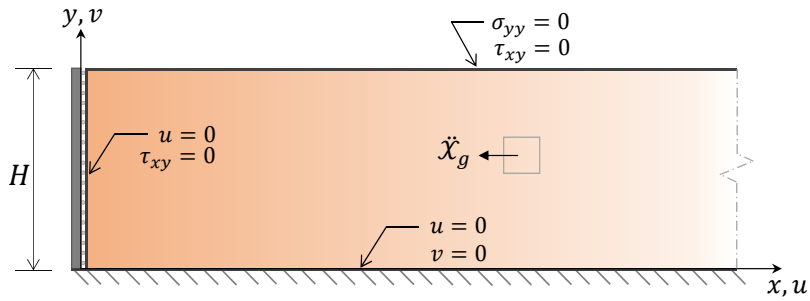

FIGURE 3 System re-framed in terms of relative displacements

$$(\lambda + 2\mu)\frac{\partial^2 u_t}{\partial x^2} + (\lambda + \mu)\frac{\partial^2 v_t}{\partial x \partial y} + \mu\frac{\partial^2 u_t}{\partial y^2} = \rho\frac{\partial^2 u_t}{\partial t^2}\,, \tag{1a}$$

$$(\lambda + 2\mu)\frac{\partial^2 v_t}{\partial y^2} + (\lambda + \mu)\frac{\partial^2 u_t}{\partial x \partial y} + \mu\frac{\partial^2 v_t}{\partial x^2} = \rho\frac{\partial^2 v_t}{\partial t^2}\,, \tag{1b}$$

subjected to the following boundary conditions:

at $y = 0$

$$u_t(x, y = 0, t) = \mathcal{X}_g(t) \qquad v_t(x, y = 0, t) = 0\,, \tag{2a}$$

while at $y = H$

$$\tau_{xy}(x, y = H, t) = 0 \qquad \sigma_{yy}(x, y = H, t) = 0\,, \tag{2b}$$

and at $x = 0$

$$\tau_{xy}(x = 0, y, t) = 0 \qquad u_t(x = 0, y, t) = \mathcal{X}_g(t)\,. \tag{2c}$$

Including hysteretic damping in the material response can be achieved by simple substitution of the real shear modulus μ by $\mu(1 + \mathrm{i}\delta_d)$, where δ_d can be referred as "damping ratio". We also assume the Poisson's ratio to be independent of damping, hence damping also affects the second elastic constant $\lambda/\mu = (1 + \mathrm{i}\delta_d)2\nu/(1 - 2\nu)$.

2.2 | Introduction of relative displacements

Both u_t and v_t represent total displacements (horizontal and vertical, respectively), measured with respect to some fixed reference. This particular problem was much more convenient to formulate in terms of relative displacements. Thus, the change of variable $u_t(x, y, t) = u(x, y, t) + \mathcal{X}_g(t)$, $v_t(x, y, t) = v(x, y, t)$ was introduced in eq. (1) to obtain the

equations of motion in terms of relative displacements:

$$(\lambda+2\mu)\frac{\partial^2 u}{\partial x^2}+(\lambda+\mu)\frac{\partial^2 v}{\partial x\,\partial y}+\mu\frac{\partial^2 u}{\partial y^2}=\rho\frac{\partial^2 u}{\partial t^2}+\rho\ddot{\mathfrak{X}}_g(t)\,, \tag{3a}$$

$$(\lambda+2\mu)\frac{\partial^2 v}{\partial y^2}+(\lambda+\mu)\frac{\partial^2 u}{\partial x\,\partial y}+\mu\frac{\partial^2 v}{\partial x^2}=\rho\frac{\partial^2 v}{\partial t^2}.\,, \tag{3b}$$

As for eq. (2a):

$$u(x,\,y=0,t)=0 \qquad v(x,\,y=0,t)=0\,, \tag{4a}$$

whereas eq. (2b) does not change insofar the stresses do not depend on the displacements themselves but on their spatial gradients:

$$\tau_{xy}(x,\,y=H,t)=0 \qquad \sigma_{yy}(x,\,y=H,t)=0\,, \tag{4b}$$

and similarly, eq. (2b) becomes

$$\tau_{xy}(x=0,\,y,t)=0 \qquad u(x=0,\,y,t)=0\,. \tag{4c}$$

Note that the original problem can be classified as “unforced wave propagation with inhomogeneous mixed boundary conditions", while this modified one corresponds to “forced wave propagation (because now there is an external body force $\rho\ddot{\mathfrak{X}}_g$ in eq. (3a)) with homogeneous mixed boundary conditions".

Purposefully, nothing has been said about initial conditions since we shall focus on steady-state response to a harmonic load. Considering a transient regime governed by the initial conditions can be achieved by appealing to Laplace's transform in time. This could be easily done, but it would entail extra muddling of the problem, as one would have to invert yet another integral transform. Moreover, such endeavor is unnecessary if we choose to focus on obtaining transfer functions connecting the external load to the response.

2.3 | Dealing with the time domain: assume harmonic loading and steady-state response

The disclosed objective of this work is, chiefly, finding the transfer function for the earth thrust on the wall. Therefore, a more-convenient, equivalent way of proceeding is to assume a harmonic decomposition of both the load and the response and, invoking superposition, focus onto one sole harmonic. In summary, this means assuming $u=\hat{u}e^{i\varpi t}$, $v=\hat{v}e^{i\varpi t}$ as well as $\ddot{\mathfrak{X}}=\ddot{X}_g e^{i\varpi t}$, where ϖ can be any excitation frequency and $\hat{u}$, $\hat{v}$ must be understood as complex numbers, whose modulus represents the magnitude of each displacement and its argument represents the phase lag between load and response. Introducing these changes into eq. (3) yields:

$$(\lambda+2\mu)\frac{\partial^2 \hat{u}}{\partial x^2}+(\lambda+\mu)\frac{\partial^2 \hat{v}}{\partial x\,\partial y}+\mu\frac{\partial^2 \hat{u}}{\partial y^2}+\rho\varpi^2\hat{u}=\rho\ddot{X}_g(t)\,, \tag{5a}$$

$$(\lambda+2\mu)\frac{\partial^2 \hat{v}}{\partial y^2}+(\lambda+\mu)\frac{\partial^2 \hat{u}}{\partial x\,\partial y}+\mu\frac{\partial^2 \hat{v}}{\partial x^2}+\rho\varpi^2\hat{v}=0\,, \tag{5b}$$

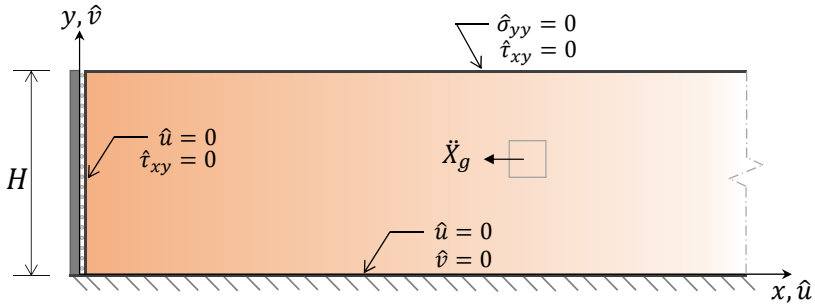

FIGURE 4 System after assuming harmonic excitation and response

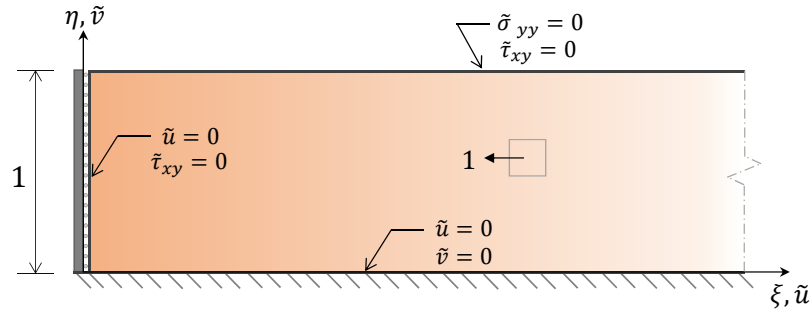

FIGURE 5 System after non-dimensionalization

with boundary conditions (from eqs. (4a) to (4c)):

$$\hat{u}(x, y = 0) = 0 \qquad \hat{v}(x, y = 0) = 0\,, \tag{6a}$$

$$\hat{\tau}_{xy}(x, y = H) = 0 \qquad \hat{\sigma}_{yy}(x, y = H) = 0\,, \tag{6b}$$

$$\hat{\tau}_{xy}(x = 0, y) = 0 \qquad \hat{u}(x = 0, y) = 0\,, \tag{6c}$$

2.4 | Nondimensionalization and key symmetry argument

Working with dimensionless equations makes it easier to keep track of the parameters of the problem and eases the burden of algebraic manipulations. Regardless of its convenience, this step is optional and does not bear any special significance within the solving procedure. For the purpose of writing the last equations in dimensionless form, the following dimensionless variables and parameters are introduced:

$$\xi = \frac{x}{H}\,, \qquad \eta = \frac{y}{H}\,, \qquad \tilde{u} = \frac{\hat{u}}{\rho \ddot{X}_g H^2/\mu}\,, \qquad \tilde{v} = \frac{\hat{v}}{\rho \ddot{X}_g H^2/\mu}\,, \qquad r = \frac{\varpi}{c_s/H}\,, \qquad c = \sqrt{\frac{\lambda + 2\mu}{\mu}}\,, \tag{7}$$

where ξ represents the dimensionless horizontal coordinate, η the dimensionless vertical coordinate, $\tilde{u}$ and $\tilde{v}$ the dimensionless horizontal and vertical displacements respectively, r the dimensionless excitation frequency, and c =

$c(\nu) = c_s/c_p = \sqrt{2(1-\nu)(1-2\nu)}$ the ratio between P-wave and S-wave propagation velocities which, in the case of isotropic linear-elastic solid, is a function of the Poisson's ratio, ν, solely. Once again, using this change of variables in eq. (5), the equations of motion become:

$$c^2 \frac{\partial^2 \tilde{u}}{\partial \xi^2} + (c^2 - 1)\frac{\partial^2 \tilde{v}}{\partial \xi \eta} + \frac{\partial^2 \tilde{u}}{\partial \eta^2} + r^2 \tilde{u} = 1\,, \tag{8a}$$

$$c^2 \frac{\partial^2 \tilde{v}}{\partial \eta^2} + (c^2 - 1)\frac{\partial^2 \tilde{u}}{\partial \xi \eta} + \frac{\partial^2 \tilde{v}}{\partial \xi^2} + r^2 \tilde{v} = 0\,, \tag{8b}$$

subject to the boundary conditions, eqs. (6a) to (6c), at $\eta = 0$:

$$\tilde{u}(\xi, \eta = 0) = 0 \quad \tilde{v}(\xi, \eta = 0) = 0\,, \tag{9a}$$

at $\eta = 1$

$$\tau_{xy}(\xi, \eta = 1) = 0 \rightarrow \frac{\partial \tilde{u}}{\partial \eta}\bigg|_{\eta=1} + \frac{\partial \tilde{v}}{\partial \xi}\bigg|_{\eta=1} = 0\,, \tag{9b}$$

$$\sigma_{yy}(\xi, \eta = 1) = 0 \rightarrow c^2 \frac{\partial \tilde{v}}{\partial \eta}\bigg|_{\eta=1} + (c^2 - 2)\frac{\partial \tilde{u}}{\partial \xi}\bigg|_{\eta=1} = 0\,, \tag{9c}$$

and at $\xi = 0$ (smooth, rigid wall)

$$\tilde{u}(\xi = 0, \eta) = 0\,, \tag{9d}$$

$$\tau_{xy}(\xi = 0, \eta) = 0 \rightarrow \frac{\partial \tilde{u}}{\partial \eta}\bigg|_{\xi=0} + \frac{\partial \tilde{v}}{\partial \xi}\bigg|_{\xi=0} = \frac{\partial \tilde{v}}{\partial \xi}\bigg|_{\xi=0} = 0\,. \tag{9e}$$

At this moment, one must consider how to deal with the unboundedness of the horizontal coordinate. Since $x \in [0, +\infty)$, an approach based on applying Laplace's transform on displacements may seem on point at first, however opting for this approach requires knowledge of both the value of the displacement and its first derivative at the wall, what is not the case: the value of $\tilde{u}$ is known yet $\partial \tilde{u}/\partial \xi$ is not, and conversely $\partial \tilde{v}/\partial \xi$ is known while $\tilde{v}$ is not. Nevertheless, the conditions seem ideal to apply Fourier sine transform and Fourier cosine transform, yet this option appears confusing as it would require using different transforms for each displacement field component.

The fitting approach for this specific problem is appealing to symmetry and then applying the classic Fourier Transform. The symmetry argument reads: this type of one-wall system formulated in terms of relative displacements, amounts to applying a symmetry condition on a infinite layer wherein the body force suddenly changes sign, but not magnitude, at $\xi = 0$.

Thus, in lieu of the semi-infinite soil strip domain, let us consider an infinite domain $\xi \in (-\infty, +\infty)$, where at $\xi = 0$ there is a discontinuity in the "loading", that is, the external body force, originally set -1 and defined over $x \geq 0$, now following a step function, $1 - 2\theta(\xi)$ defined over $x \in \mathbb{R}$, where $\theta(\xi)$ is the Heaviside function centered at $\xi = 0$.

Hence, the system that will finally be solved is governed by the following equations and boundary conditions (equivalent to eq. (8) with boundary conditions (9)):

$$c^2 \frac{\partial^2 \tilde{u}}{\partial \xi^2} + (c^2 - 1)\frac{\partial^2 \tilde{v}}{\partial \xi \eta} + \frac{\partial^2 \tilde{u}}{\partial \eta^2} + r^2 \tilde{u} = 2\theta(\xi) - 1\,, \tag{10a}$$

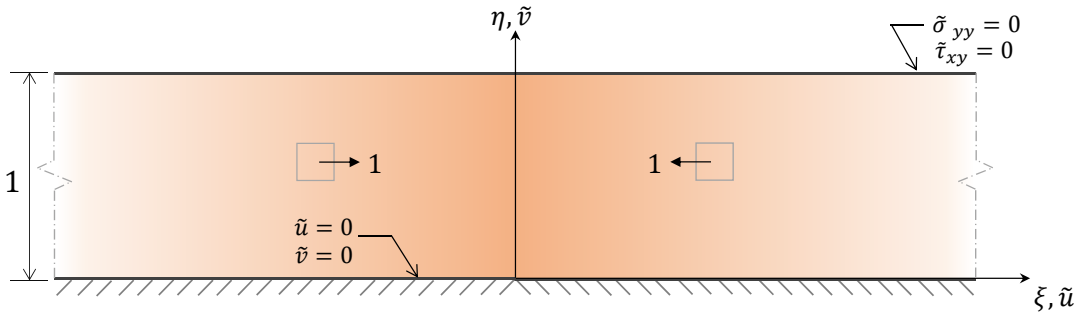

FIGURE 6 Nondimensional system after applying symmetry argument

$$c^2\frac{\partial^2\tilde{v}}{\partial\eta^2}+(c^2-1)\frac{\partial^2\tilde{u}}{\partial\xi\eta}+\frac{\partial^2\tilde{v}}{\partial\xi^2}+r^2\tilde{v}=0\,, \tag{10b}$$

subject to the boundary conditions at $\eta = 0$:

$$\tilde{u}(\xi,\eta=0)=0\quad\tilde{v}(\xi,\eta=0)=0\,, \tag{11a}$$

at $\eta = 1$

$$\tau_{xy}(\xi,\eta=1)=0\rightarrow\frac{\partial\tilde{u}}{\partial\eta}\bigg|_{\eta=1}+\frac{\partial\tilde{v}}{\partial\xi}\bigg|_{\eta=1}=0\,, \tag{11b}$$

$$\sigma_{yy}(\xi,\eta=1)=0\rightarrow c^2\frac{\partial\tilde{v}}{\partial\eta}\bigg|_{\eta=1}+(c^2-2)\frac{\partial\tilde{u}}{\partial\xi}\bigg|_{\eta=1}=0\,. \tag{11c}$$

We resort to the Fourier Transform [21] at this point:

$$F[\tilde{u}]=\frac{1}{\sqrt{2\pi}}\int_{-\infty}^{+\infty}\tilde{u}e^{ik\xi}d\xi=U\,, \tag{12a}$$

$$F[\tilde{v}]=\frac{1}{\sqrt{2\pi}}\int_{-\infty}^{+\infty}\tilde{v}e^{ik\xi}d\xi=V\,, \tag{12b}$$

where k is the dimensionless horizontal wavenumber (its relation to the physical wavenumber k being $kH = k$), hence eq. (10) becomes

$$ik(c^2-1)\frac{\partial V}{\partial\eta}+\frac{\partial^2U}{\partial\eta^2}+(r^2-c^2k^2)U-\sqrt{\frac{2}{\pi}}\frac{i}{k}=0\,, \tag{13a}$$

$$c^2\frac{\partial^2V}{\partial\eta^2}+ik(c^2-1)\frac{\partial U}{\partial\eta}+(r^2-k^2)V=0\,, \tag{13b}$$

likewise, eq. (11) becomes the following:

at $\eta = 0$

$$U(0) = 0 \quad V(0) = 0\,, \tag{14a}$$

at $\eta = 1$

$$\tau_{xy} = 0 \rightarrow \frac{\partial U}{\partial \eta}\Big|_{\eta=1} + ikV = 0\,, \tag{14b}$$

$$\sigma_{yy} = 0 \rightarrow c^2 \frac{\partial V}{\partial \eta}\Big|_{\eta=1} + ik(c^2 - 2)U = 0.\,, \tag{14c}$$

Equation 14 represents the problem in the original vertical (nondimensional) variable and in the wavenumber (k) domain, assuming harmonic loading and steady-state conditions.

2.5 | Exact solution in the horizontal wavenumber space

The system of equations (13) can be even more condensed by introducing additional auxiliary variables $\mathcal{V} = \partial V/\partial \eta$, $\mathcal{U} = \partial U/\partial \eta = \partial[U - (k(r^2 - c^2k^2))^{-1}]/\partial \eta$:

$$\frac{\partial \mathcal{U}}{\partial \eta} = ik(1 - c^2)\mathcal{V} + (c^2k^2 - r^2)\left(U + \sqrt{\frac{2}{\pi}}\frac{i}{k(c^2k^2 - r^2)}\right), \tag{15a}$$

$$\frac{\partial}{\partial \eta}\left(U + \sqrt{\frac{2}{\pi}}\frac{i}{k(c^2k^2 - r^2)}\right) = \mathcal{U}\,, \tag{15b}$$

$$\frac{\partial \mathcal{V}}{\partial \eta} = ik\frac{(1 - c^2)}{c^2}\mathcal{U} + \frac{(k^2 - r^2)}{c^2}V\,, \tag{15c}$$

$$\frac{\partial V}{\partial \eta} = \mathcal{V}\,, \tag{15d}$$

subject to the boundary conditions equivalent to (14):

at $\eta = 0$

$$U(0) = 0 \quad V(0) = 0\,, \tag{16a}$$

at $\eta = 1$

$$\mathcal{U}(1) = -ikV(1)\,, \tag{16b}$$

$$c^2\mathcal{V}(1) = -ik(c^2 - 2)U(1)\,. \tag{16c}$$

Introducing a vector of unknowns, $\boldsymbol{X} = \begin{bmatrix} \mathcal{U} & U + \sqrt{\frac{2}{\pi}} \frac{i}{k(c^2k^2 - r^2)} & \mathcal{V} & V \end{bmatrix}^T$, eq. (15) can be written simply as

$$\boldsymbol{X}' = \boldsymbol{D}\boldsymbol{X}\,, \tag{17}$$

where

$$\boldsymbol{D} = \begin{bmatrix} 0 & (c^2k^2 - r^2) & ik(1-c^2) & 0 \\ 1 & 0 & 0 & 0 \\ ik\frac{(1-c^2)}{c^2} & 0 & 0 & \frac{(k^2-r^2)}{c^2} \\ 0 & 0 & 1 & 0 \end{bmatrix}. \tag{18}$$

The eigenvalues of this matrix are

$$\lambda_1 = -\sqrt{k^2 - r^2}\,, \quad \lambda_2 = \sqrt{k^2 - r^2}\,, \quad \lambda_3 = -\sqrt{k^2 - (r/c)^2}\,, \quad \lambda_4 = \sqrt{k^2 - (r/c)^2}\,, \tag{19}$$

where each solution corresponds to S-waves (first two solutions) and P-waves (last two solutions) propagating within the bulk of the stratum. Since we do not pursue the inversion of the solution in this paper, we shall not delve in the intrincacies of properly choosing branches of this multi-valued function [22]. The eigenvectors (normalized to 1 in the fourth entry) are

$$\varphi_1 = \begin{bmatrix} i\frac{(k^2-r^2)}{k} \\ -i\frac{(\sqrt{k^2-r^2})}{k} \\ -\sqrt{k^2 - r^2} \\ 1 \end{bmatrix}, \quad \varphi_2 = \begin{bmatrix} i\frac{(k^2-r^2)}{k} \\ i\frac{(\sqrt{k^2-r^2})}{k} \\ \sqrt{k^2 - r^2} \\ 1 \end{bmatrix}, \quad \varphi_3 = \begin{bmatrix} ik \\ -i\frac{k}{\sqrt{k^2-(r/c)^2}} \\ -\sqrt{k^2 - (r/c)^2} \\ 1 \end{bmatrix}, \quad \varphi_4 = \begin{bmatrix} ik \\ i\frac{k}{\sqrt{k^2-(r/c)^2}} \\ \sqrt{k^2 - (r/c)^2} \\ 1 \end{bmatrix}, \tag{20}$$

thus the solution must be

$$\begin{aligned} \boldsymbol{X} = \begin{bmatrix} \mathcal{U} \\ U + \sqrt{\frac{2}{\pi}} \frac{i}{k(c^2k^2-r^2)} \\ \mathcal{V} \\ V \end{bmatrix} = & A \begin{bmatrix} i\frac{(k^2-r^2)}{k} \\ -i\frac{(\sqrt{k^2-r^2})}{k} \\ -\sqrt{k^2 - r^2} \\ 1 \end{bmatrix} e^{-\sqrt{k^2-r^2}\eta} + B \begin{bmatrix} i\frac{(k^2-r^2)}{k} \\ i\frac{(\sqrt{k^2-r^2})}{k} \\ \sqrt{k^2 - r^2} \\ 1 \end{bmatrix} e^{\sqrt{k^2-r^2}\eta} \\ & + C \begin{bmatrix} ik \\ -i\frac{k}{\sqrt{k^2-(r/c)^2}} \\ -\sqrt{k^2 - (r/c)^2} \\ 1 \end{bmatrix} e^{-\sqrt{k^2-(r/c)^2}\eta} + D \begin{bmatrix} ik \\ i\frac{k}{\sqrt{k^2-(r/c)^2}} \\ \sqrt{k^2 - (r/c)^2} \\ 1 \end{bmatrix} e^{\sqrt{k^2-(r/c)^2}\eta}, \end{aligned} \tag{21}$$

or introducing the following shorthands $\alpha = \sqrt{k^2 - r^2}$, $\beta = \sqrt{k^2 - (r/c)^2}$:

$$\boldsymbol{X} = \begin{bmatrix} \mathcal{U} \\ U + \sqrt{\frac{2}{\pi}} \frac{i}{c^2k\beta^2} \\ \mathcal{V} \\ V \end{bmatrix} = A \begin{bmatrix} i\frac{\alpha^2}{k} \\ -i\frac{\alpha}{k} \\ -\alpha \\ 1 \end{bmatrix} e^{-\alpha\eta} + B \begin{bmatrix} i\frac{\alpha^2}{k} \\ i\frac{\alpha}{k} \\ \alpha \\ 1 \end{bmatrix} e^{\alpha\eta} + C \begin{bmatrix} ik \\ -i\frac{k}{\beta} \\ -\beta \\ 1 \end{bmatrix} e^{-\beta\eta} + D \begin{bmatrix} ik \\ i\frac{k}{\beta} \\ \beta \\ 1 \end{bmatrix} e^{\beta\eta}, \tag{22}$$

where A, B, C, D are "constants" (which nevertheless depend on the parameter k) to be determined from the boundary conditions, starting from the easiest ones, $V(0) = 0$ and $U(0) = 0$

$$V(0) = A + B + C + D = 0\,, \tag{23}$$

$$U(0) = \frac{i\alpha}{k}(B - A) + \frac{ik}{\beta}(D - C) - \sqrt{\frac{2}{\pi}}\frac{i}{c^2 k\beta^2} = 0\,, \tag{24}$$

followed by the most convoluted conditions at $\eta = 1$, $\tau_{xy} = 0$

$$\mathcal{U}(1) + ikV(1) = 0 \rightarrow \frac{i\alpha^2}{k}(Ae^{-\alpha} + Be^{\alpha}) + ik(Ce^{-\beta} + De^{\beta}) = 0 \rightarrow \tag{25a}$$

$$ik(Ae^{-\alpha} + Be^{\alpha}) + ik(Ce^{-\beta} + De^{\beta}) = 0 \rightarrow \tag{25b}$$

$$\left(k + \frac{\alpha^2}{k}\right)(Ae^{-\alpha} + Be^{\alpha}) + 2k(Ce^{-\beta} + De^{\beta}) = 0\,, \tag{25c}$$

and $\sigma_{yy} = 0$

$$c^2\mathcal{V}(1) + ik(c^2 - 2)\left(U(1) \pm \sqrt{\frac{2}{\pi}}\frac{i}{c^2 k\beta^2}\right) = 0 \rightarrow \tag{26a}$$

$$\begin{aligned} &c^2\mathcal{V}(1) + ik(c^2 - 2)\left(U(1) + \sqrt{\frac{2}{\pi}}\frac{i}{c^2 k\beta^2}\right) = -\sqrt{\frac{2}{\pi}}\frac{(c^2 - 2)}{c^2\beta^2} = \\ &= c^2\alpha(Be^{\alpha} - Ae^{-\alpha}) + c^2\beta(De^{\beta} - Ce^{-\beta}) \\ &\quad - (c^2 - 2)\alpha(Be^{\alpha} - Ae^{-\alpha}) - (c^2 - 2)\frac{k^2}{\beta}(De^{\beta} - Ce^{-\beta}) = \\ &= 2\alpha(Be^{\alpha} - Ae^{-\alpha}) + \left(\frac{c^2(\beta^2 - k^2) + 2k^2}{\beta}\right)(De^{\beta} - Ce^{-\beta})\,. \end{aligned} \tag{26b}$$

Recast eqs. (23), (24), (25c) and (26b) in matrix form:

$$\begin{bmatrix} 1 & 1 & 1 & 1 \\ -\frac{i\alpha}{k} & \frac{i\alpha}{k} & -\frac{ik}{\beta} & \frac{ik}{\beta} \\ \left(k + \frac{\alpha^2}{k}\right)e^{-\alpha} & \left(k + \frac{\alpha^2}{k}\right)e^{\alpha} & 2ke^{-\beta} & 2ke^{\beta} \\ -2\alpha e^{-\alpha} & 2\alpha e^{\alpha} & -\left(\frac{c^2(\beta^2 - k^2) + 2k^2}{\beta}\right)e^{-\beta} & \left(\frac{c^2(\beta^2 - k^2) + 2k^2}{\beta}\right)e^{\beta} \end{bmatrix} \begin{bmatrix} A \\ B \\ C \\ D \end{bmatrix} = \begin{bmatrix} 0 \\ \sqrt{\frac{2}{\pi}}\frac{i}{c^2 k\beta^2} \\ 0 \\ -\sqrt{\frac{2}{\pi}}\frac{(c^2 - 2)}{c^2\beta^2} \end{bmatrix}, \tag{27}$$

the value of the constants is found after solving (inverting) this linear system. The actual expressions are computed by recourse to *Mathematica* [23]. The expressions are frankly convoluted, so denominator and numerator are shown separately. For instance, the coefficient A is expressed as $A = A_N/A_D$. Therefore:

$$\begin{aligned} A_N = &- e^{\alpha}\alpha^2\left(e^{2\beta} + 1\right)\beta^2 c^2 + \left(e^{\alpha} + 2\right)\left(e^{\beta} - 1\right)^2\left(c^2 - 2\right)k^4 + k^2\Big[e^{\alpha}\left(-4\alpha\beta + \alpha^2\left(c^2 - 2\right) - \beta^2 c^2\right) + \\ &+ e^{\alpha+2\beta}\left(4\alpha\beta + \alpha^2\left(c^2 - 2\right) - \beta^2 c^2\right) - 2\alpha^2\left(c^2 - 2\right)e^{\alpha+\beta} + 2\alpha e^{2\beta}\beta\left(c^2 - 2\right) - 2\alpha\beta\left(c^2 - 2\right) + 4e^{\beta}\beta^2 c^2\Big]\,, \end{aligned} \tag{28a}$$

$$\begin{aligned} B_N = &e^{-\alpha-\beta}\Big[k^2\left(\alpha^2\left(e^{\beta} - 1\right)^2\left(2 - c^2\right) + \beta^2 c^2\left(-4e^{\alpha+\beta} + e^{2\beta} + 1\right) + 2\alpha\left(e^{2\beta} - 1\right)\beta\left(e^{\alpha}\left(c^2 - 2\right) + 2\right)\right) + \\ &+ \alpha^2\left(e^{2\beta} + 1\right)\beta^2 c^2 + \left(2e^{\alpha} + 1\right)\left(e^{\beta} - 1\right)^2\left(2 - c^2\right)k^4\Big]\,, \end{aligned} \tag{28b}$$

$$C_N = 2\alpha\beta\left[\alpha^2 + k^2\left(1 - e^{\beta}\left(c^2 - 2\right)\right)\right] - \sinh(\alpha)\left(\alpha^2 + k^2\right)\left[\left(e^{\beta} - 1\right)\left(c^2 - 2\right)k^2 - e^{\beta}\beta^2 c^2\right] \tag{28c}$$

$$+ \alpha\beta\cosh(\alpha)\left[\left(c^2 - 2\right)\left(\alpha^2 + k^2\right) - 4e^{\beta}k^2\right], \tag{28d}$$

$$D_N = e^{-\alpha-\beta}\Big[\alpha^2\beta\left(\left(e^{2\alpha} - 1\right)\beta c^2 - 2\alpha e^{\alpha+\beta}\left(\left(c^2 - 2\right)\cosh(\alpha) + 2\right)\right) + \left(e^{2\alpha} - 1\right)\left(e^{\beta} - 1\right)\left(c^2 - 2\right)k^4 +$$

$$+ k^2\Big(4\alpha\beta + \left(e^{2\alpha} - 1\right)\alpha^2\left(e^{\beta} - 1\right)\left(c^2 - 2\right) - 2e^{\alpha}\alpha\beta\left(e^{\beta}\left(\left(c^2 - 2\right)\cosh(\alpha) + 2\right) - 2\left(e^{\alpha} + c^2 - 2\right)\right)$$

$$+ \left(e^{2\alpha} - 1\right)\beta^2 c^2\Big)\Big], \tag{28e}$$

and the corresponding denominators:

$$A_D = \sqrt{2\pi}\beta c^2\Big[\alpha\left(e^{2\beta} + 1\right)\beta\cosh(\alpha)\left(\left(6 - c^2\right)k^4 + \beta^2 c^2\left(\alpha^2 + k^2\right) - \alpha^2\left(c^2 - 2\right)k^2\right) +$$

$$+ 2e^{\beta}k^2\left(\sinh(\alpha)\sinh(\beta)\left(\left(c^2 - 2\right)k^2\left(\alpha^2 + k^2\right) - \beta^2\left(\alpha^2\left(c^2 + 4\right) + c^2k^2\right)\right) - 2\alpha\beta\left(\alpha^2 + \beta^2c^2 + \left(3 - c^2\right)k^2\right)\right)\Big], \tag{29a}$$

$$B_D = 2\sqrt{2\pi}\beta c^2\Big[\alpha\beta\cosh(\alpha)\cosh(\beta)\left(\left(6 - c^2\right)k^4 + \beta^2c^2\left(\alpha^2 + k^2\right) - \alpha^2\left(c^2 - 2\right)k^2\right)$$

$$+ k^2\left(\sinh(\alpha)\sinh(\beta)\left(\left(c^2 - 2\right)k^2\left(\alpha^2 + k^2\right) - \beta^2\left(\alpha^2\left(c^2 + 4\right) + c^2k^2\right)\right) - 2\alpha\beta\left(\alpha^2 + \beta^2c^2 + \left(3 - c^2\right)k^2\right)\right)\Big], \tag{29b}$$

$$C_D = B_D/2, \tag{29c}$$

$$D_D = B_D. \tag{29d}$$

There is no tabulated formula to invert the integrals where the coefficients appear. Analytical inversions must be performed by recourse to Contour Integration and Residue Calculus [22], which turns out to be an extensive and challenging task that the authors have not succeeded in yet.

3 | EVALUATING AND VERIFYING THE SOLUTION

Instead of taking that path, one can approximate the integral numerically, as the coefficients can be easily evaluated in *Mathematica*. To approximate this integral numerically, the integration has to be stopped at some point; it is known (from previous study carried out by the first author in the context of his doctoral thesis [24]) that the horizontal wavelengths $\sim H$ are those that control the response close to the wall, and are also the shortest wavelengths that are present. Therefore, one can limit the integration to $|k| \in [0, 10]$.

Once these coefficients have been computed, the solution in the wavenumber domain has been found. Results derived from the exact solution are compared to FEM analysis performed on *Abaqus* [25]. This package, at the time the simulations were run, does not contain elements suitable to model *open boundaries* [26]. For this reason, as the unboundedness in the horizontal direction can not be accounted formally, a very slender model of length L ($L/H = 275/2$) was used. This approach mirrors the one advocated recently by Durante and collaborators [27], which delivered satisfactory results in the quasi-static regime, yet it had not been tested in frequency-domain dynamic analysis previously.

The parameter models are encapsulated in the following table. Keep in mind that *Abaqus* does not work with units, it is the responsibility of the user to keep track of them if necessary, and that this is not a concern since we are

dealing with a linear problem and all the results will be turned dimensionless.

Young's modulus	Density	Height	Acceleration
E	ρ	H	$\ddot{X}_g$
10^9	2000	2	0.73

TABLE 1 Parameters used in finite-element simulations

The details on the analyses carried out in *Abaqus* follow:

- First step: "Frequency" analysis uses the Lanczos method to extract the resonance modes in the interval $[0, 500]$ cycles per time unit (this range is chosen so as to capture the first modes of the corresponding shear beam given the parameter values in Table 1). The frequency domain is uniformly subdivided using 1000 points.
- Second step: "Steady-state Dynamics - Modal" analysis: using the newly obtained information on the natural frequencies of the system, the transfer function, in that frequency range, for the any response is obtained.

3.1 | Vertical displacement at upper-left corner

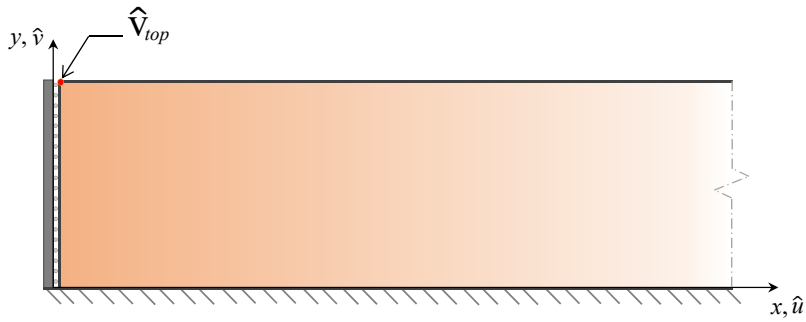

FIGURE 7 Probe location for $\tilde{\mathrm{v}}_{top}$

One can then move to calculate, for instance, the vertical displacement at the top of the wall, $\tilde{v}(\eta = 1, \xi = 0) = \tilde{\mathrm{v}}_{top}$, by inverting the transform:

$$\tilde{\mathrm{v}}_{top} = F^{-1}[V]_{\eta=1,\xi=0} = \frac{1}{\sqrt{2\pi}} \int_{-\infty}^{+\infty} \left[V e^{-ik\xi} \right]_{\eta=1,\xi=0} dk \,, \tag{30a}$$

recall $V = Ae^{-\alpha\eta} + Be^{\alpha\eta} + Ce^{-\beta\eta} + De^{\beta\eta}$,

$$= \frac{1}{\sqrt{2\pi}} \int_{-\infty}^{+\infty} \left[Ae^{-\alpha} + Be^{\alpha} + Ce^{-\beta} + De^{\beta} \right] dk \,, \tag{30b}$$

where A, B, C, D, α, and β are functions of the dimensionless wavenumber k, and the integration is limited to $k \in [-10, 10]$.

The comparison of eq. (30b), as evaluated in *Mathematica*, to the results obtained in *Abaqus*, once properly expressed in non-dimensional form, is displayed in Figures 8 and 9. The characteristic displacement $U = \rho \ddot{X}_g H^2/\mu$ is the

same that was used to write displacements in dimensionless form in (7). The first plot corresponds to $\delta_d = 0.05$ and the second one to $\delta_d = 0.16$, and in both bases $\nu = 0.1$ and $r = \pi\varpi/2\omega_s \in [0, 5\pi/4]$, $\omega_s = \pi c_s/2H$.

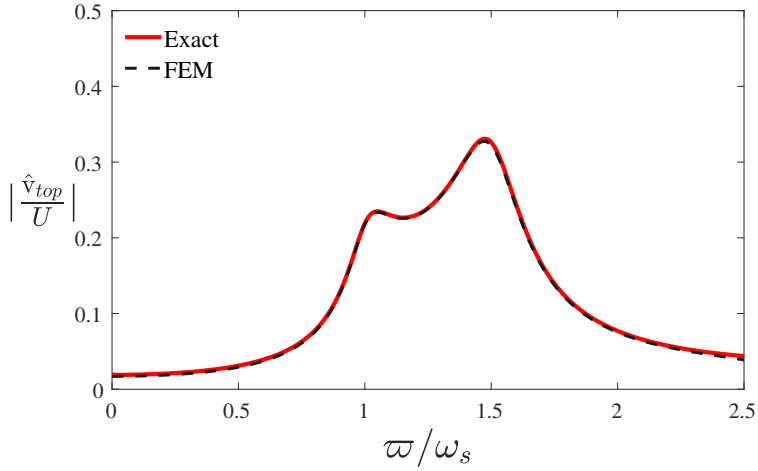

FIGURE 8 Transfer function for the vertical displacement at the top of the wall, $\nu = 0.1$, $\delta_d = 0.16$

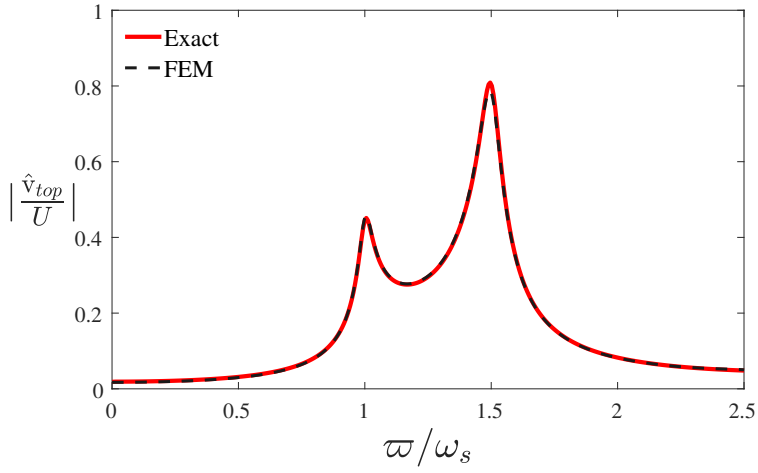

FIGURE 9 Transfer function for the vertical displacement at the top of the wall, $\nu = 0.1$, $\delta_d = 0.05$

Both analytical and numerical estimations of Figure 8 and Figure 9 were found to be in excellent agreement. It must be highlighted that, for $\nu = 0.1$ we observe a second resonance, not present in the far-field response, at $\varpi \approx 1.5\omega_s = c\,\omega_s = \omega_p$, since $c = c_p/c_s = 1.5$ when $\nu = 0.1$.

3.2 | Earth thrust over the wall

The earth thrust represents the integral of the stresses that develop at the soil-wall interface. In the case of the smooth wall, harmonic loading and steady-state conditions, it can be written as

$$Q = \hat{Q}e^{i\varpi t} = e^{i\varpi t}\int_0^H \hat{\sigma}_{xx}(x=0,y)\,dy\,, \tag{31}$$

ergo the amplitude of the thrust can be expressed in terms of the solution coefficients in the vhorizontal wavenumber domain as the inverse Fourier transform below:

$$\frac{\hat{Q}}{\rho\ddot{X}_g H^2} = \frac{1}{\sqrt{2\pi}}\int_{-\infty}^{+\infty}\left\{\frac{\sqrt{2/\pi}}{\beta^2} + c^2(A+B) - 2(Ae^{-\alpha} + Be^{\alpha}) + \left[c^2\left(1-\left(\frac{k}{\beta}\right)^2\right) - 2\right]\left(Ce^{-\beta} + De^{\beta}\right) + \left(\frac{ck}{\beta}\right)^2 (C+D)\right\}dk. \tag{32}$$

Similarly to eq. (30b), the equation can be evaluated numerically.

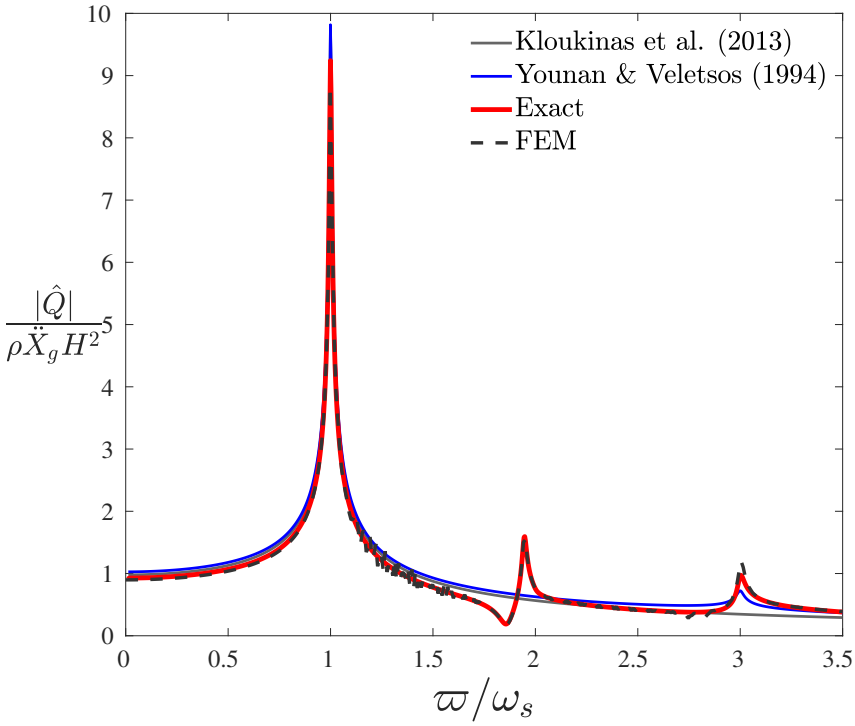

FIGURE 10 Transfer function for the earth thrust the wall, $\nu = 1/3$, $\delta_d = 0.01$, including comparison to previous engineering solutions in [13] and [17].

For $\nu = 1/3$ and $\delta_d = 0.01$, see Figure 10. The plot includes numerical results from eq. (32) in *Mathematica* and two previous research results: the thrust provided by Younan and Veletos [13] (evaluated using the five first modes), based on the assumption $\sigma_{yy} = 0$, and its direct state-of-the-art heir by Kloukinas and colleagues [17], which considers

only the fundamental mode. There seems to be some numerical artifact the authors have not yet identified, which makes the numerical result oscillate mildly between the first two spikes. Other than that, the agreement is practically excellent (there is a meager mismatch of amplitudes at the first and third resonant spikes). All the features predicted by the exact solution are present in the FEM analysis, including a substantive "dip" (deamplification) right before the second peak. As reported in Figure 8 and Figures thereafter, this resonance happens at $\varpi \approx 2\omega_s = c\,\omega_s = \omega_p$, since $c_p/c_s = 2$ as $\nu = 1/3$. This secondary resonance would have been overlooked had we assumed the thrust resonates at the same natural frequencies as the 1D soil column in the far-field [13].

The effect of damping on the thrust is addressed in Figure 11. The figures correspond to $\nu = 0.1$ (so one should expect, again, to find resonance at $\varpi/\omega_s = 1, 1.5, 3$ and so on), three different increasing values of damping are used $\delta_d = 0.05, 0.1, 0.2$,, and, again, $r = \pi\varpi/2\omega_s \in [0\,, 7\pi/4]$.

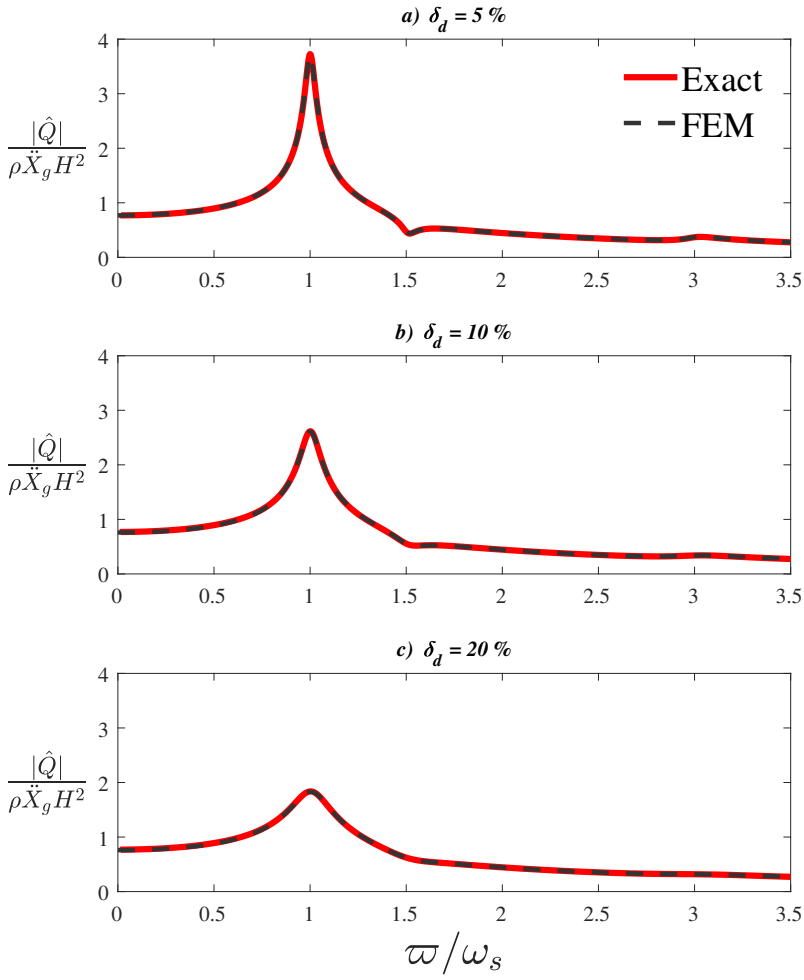

FIGURE 11 Transfer function for the earth thrust the wall, $\nu = 0.1$, $\delta_d = 0.05, 0.1, 0.2$

Again, there is an excellent compliance of numerical to analytical results, in the three cases. It is instructive to

note that in this case, $\nu = 0.1$, the dent at the "intermediate resonance" seems not to point up but down and that increasing damping smooths out the two second resonant peaks and the aforementioned dip that happens before the resonance associated with ω_p. The physical meaning of this "intermediate" resonance has yet to be described: it remains to demonstrate if it is an artifact of mode conversion or of a surface wave propagating along the wall-soil interface, and how pernicious its effects can be over the wall integrity. Something is sure: it had been unaccounted for in the previous engineering solutions, which only displayed resonance at the wall at the same natural frequencies as the far-field.

3.2.1 | In-depth analysis of intermediate resonance

This section is aimed to explain the causes of the extra set of resonance frequencies. Let us begin by noting that the normal horizontal stress developing at the soil-wall interface, and the thrust itself by extension, can be decomposed in two parts. From eq. (31), introducing the linear-elastic constitutive law,

$$\hat{Q} = \int_0^H \hat{\sigma}_{xx}(x=0,y)\,dy = \int_0^H \left[(\lambda+2\mu)\frac{\partial \hat{u}}{\partial x} + \lambda\frac{\partial \hat{v}}{\partial y}\right]_{x=0} dy = (\lambda+2\mu)\int_0^H \frac{\partial \hat{u}}{\partial x}\Big|_{x=0} dy + \lambda \hat{v}_{top}\,, \tag{33a}$$

and writing it in dimensionless form as in eq. (32):

$$\frac{\hat{Q}}{\rho \ddot{X}_g H^2} = c^2 \int_0^1 \frac{\partial \tilde{u}}{\partial \xi}\Big|_{\xi=0} d\eta + (c^2-2)\tilde{v}_{top}\,. \tag{33b}$$

The first addend corresponds to the stress induced by gradients of horizontal displacement, viz. the straining of the soil bordering the wall in the horizontal direction. The second corresponds to the gradients of vertical displacement over the wall, viz. the straining along the vertical direction. See how in previous engineering solutions [13, 17] both components were linked through the simplifying assumption $\sigma_{yy} = 0$, which forces them to have the same phase in all the cases, regardless of excitation frequency or Poisson's ratio of the soil, and also linked their amplitude through the so-called "compressibility" factor. The exact solution renders a more complex picture, wherein the two components are independent and behave significantly differently. Let us showcase this.

We already have $\tilde{v}_{top}$ expressed in terms of an inverse Fourier transform of the coefficients, eq. (30b), similarly the integral over the wall of the horizontal gradient of the horizontal displacement can be expressed as

$$\int_0^1 \frac{\partial \tilde{u}}{\partial \xi}\Big|_{\xi=0} d\eta = \frac{1}{\sqrt{2\pi}} \int_{-\infty}^{+\infty} \left\{ \frac{\sqrt{2/\pi}}{c^2\beta^2} - A(e^{-\alpha}-1) - B(e^{\alpha}-1) + \left(\frac{k}{\beta}\right)^2 \left[(C(e^{-\beta}-1) + D(e^{\beta}-1) \right] \right\} dk\,. \tag{34}$$

Recall that the inertial force oriented towards the wall (e.g. towards the negative abscissa) in Section 2.2 is just a proxy for the imposed movement along positive abscissa in Section 2.1 that appeared when making the change of variable from total to relative displacements. Hence, the compressive force induces always a relative displacement towards the wall, thus the baseline displacement is negative and its phase corresponds to zero at low-frequency since this negative displacement is in phase with a negative force. Nevertheless, the direction of the vertical displacement does depend on the compressibility of the soil: in the case $\nu = 0.1$ the soil slides down compressing the soil at the interface vertically, whereas in the case $\nu = 1/3$ the soil slides up, stretching it. The threshold value from one behavior to the other (the one corresponding to no vertical displacement whatsoever) seems to be $\nu = 0.15$. This is easy to visualize attending to the low-frequency response (quasi-static regime, corresponding to $\varpi/\omega_s << 1$) as depicted in Figure 12:

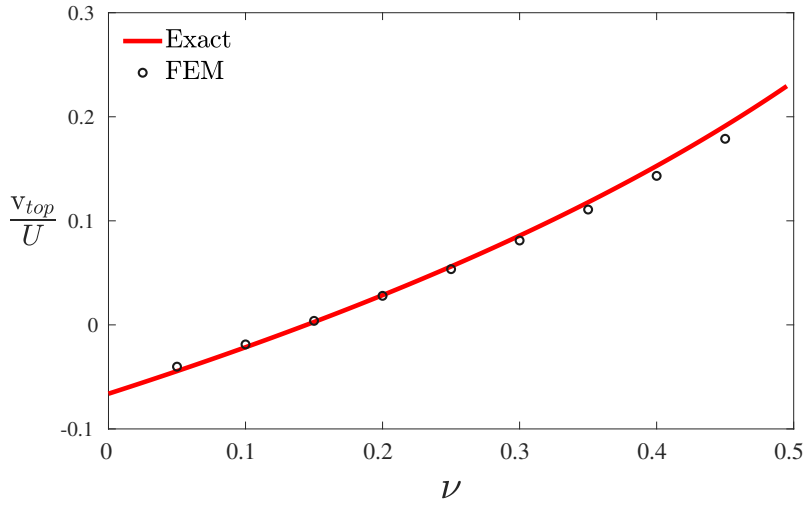

FIGURE 12 Low-frequency vertical displacement at the top of the wall for different values of Poisson's ratios

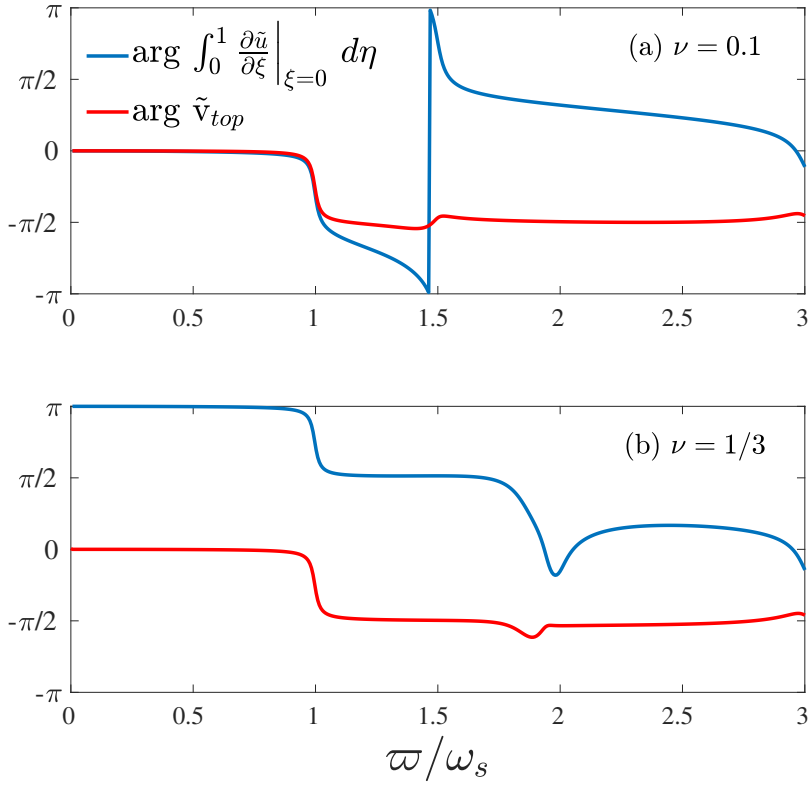

FIGURE 13 Phase of the vertical displacement at the top of the wall, given by eq. (30b), and of the integral over the wall of the horizontal gradient of horizontal displacement, given by eq. (34), for two values of the Poisson's ratio, one at each side of the threshold value. Damping $\delta_d = 0.03$ in both cases.

We posit that each component plays a different role in furnishing the total thrust, and that the phase lag between the two is a critical factor. In order to check this assertion, the phase of the two addends in eq. (33b), eqs. (30b) and (34), is compared next using the analytical solution (see Figure 13).

We acknowledge that the vertical displacement at the top corner of the layer is in phase with the horizontal gradient of horizontal displacement when $\nu = 0.1$, hence, once the second resonance frequency is excited the phase lag between the two is so big that the contribution of v_{top}, which clearly increases more due to this resonance, diminishes the total amplitude of the two combined addends. Conversely, in the case $\nu = 1/3$, the vertical displacement is positive when the horizontal displacement gradient is negative, hence the former is delayed π radians, half a period, with respect to the latter; nevertheless, when the second resonance frequency is excited, both components contribute positively to the response as both their phases have the same sign.

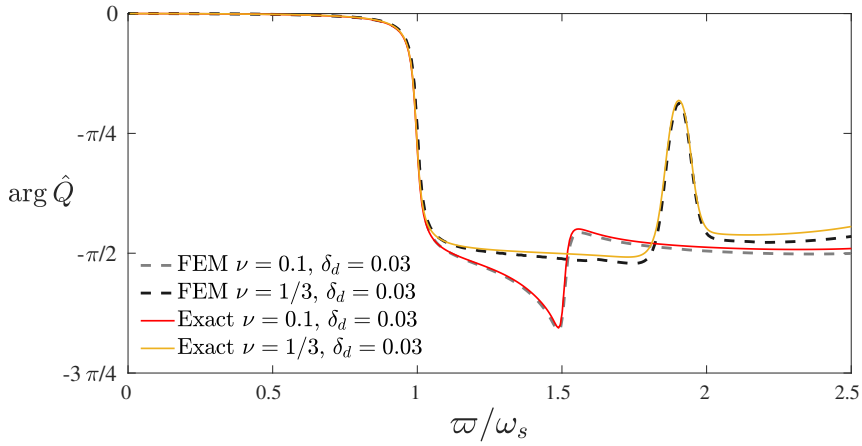

FIGURE 14 Comparison thrust phase for $\nu = 0.1$ (below the threshold $\nu \approx 0.15$) and for $\nu = 1/3$ (above the threshold). In all cases $\delta_d = 0.03$.

In conclusion, the appearance of the new resonant spikes and their different amplitude that depend on the compressibility of the soil (the Poisson's ratio) is elicited by the different behavior of the two components of the thrust on the wall –one proportional to the integral over the wall of the horizontal gradient of the horizontal displacement, eq. (34), and the other to the vertical displacement at the top of the layer, eq. (30b))– which resonate at different frequencies, and the relative delay (phase lag) between them.

3.2.2 | Simultaneous resonance

It has already been discussed that there are two contributions to the thrust, each with different features:

- One component that depends on the integral over the wall of the horizontal gradient of horizontal displacement, eq. (34), which resonates at the same frequencies as the far-field, odd multiples of $\omega_s = \pi c_s/2/H$.
- A second component proportional to the vertical displacement at the top of the layer, v_{top}, which resonates at the same frequencies as the far-field (just like the prior term) *and* at a second set of frequencies corresponding to odd multiples of $\omega_p = \pi c_p/2/H = \pi c(\nu)c_s/2/H = c(\nu)\omega_s$. At each frequency, the lag between the second and

first components depend on the compressibility of the soil.

Previous engineering results [13, 17, 28] only captured the first set of resonances. Assume that we are to consider a set of different soils having the same density, ρ, and shear stiffness, μ, but different compressibility, ν, the location of the first of set of natural frequencies, those that coincide with the "shear beam" resonance modes which are proportional to ω_s, is the same for every instance, but the location of the second set of frequencies will depend on the value of Poisson's ration through the factor $c(\nu) = c_p/c_s = \sqrt{2(1-\nu)/(1-2\nu)}$.

See that if $\nu = 7/16 = 0.4375$, then $c = 3$, whence $\omega_p = 3\omega_s$: the first resonance mode of the second set coincides with the second mode of the first set. This happens above the aforesaid threshold $\nu \approx 0.15$, thus, based on the discussion in the previous section, the two contributions of the thrust reinforce each other.

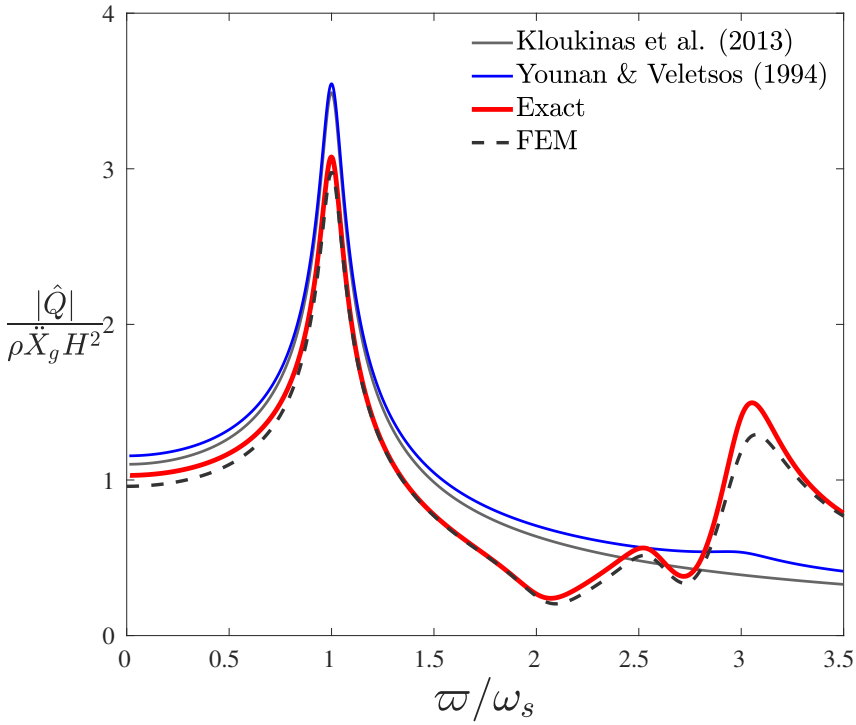

FIGURE 15 Transfer function for the earth thrust the wall, $\nu = 7/16$, $\delta_d = 0.1$, including comparison to previous engineering solutions in [13] and [17].

Figure 15 displays the unconservative limitations of prior approximate solutions: even though the the amplitude of the first peak is even slightly overestimated, the second resonance, which in this case includes also the first peak corresponding to the second set of modes, is overlooked.

This simultaneous resonances are not restricted to a narrow band of values of ν around 0.4375 but it happens for other values. Figure 16 displays a comparison between $0.42, 0.4375, 0.45$. In all three cases remarkable increments with respect to the values delivered by the engineering approximations are found in the region surrounding $\varpi \approx 3\omega_s$.

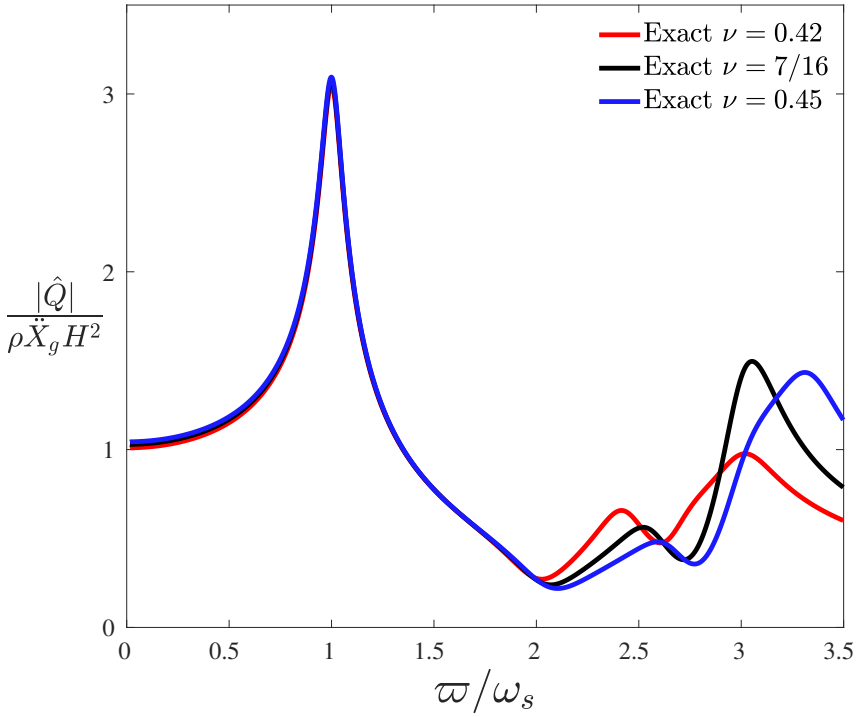

FIGURE 16 Transfer function for the earth thrust the wall for three values of ν (0.42, 0.4375, 0.45) and $\delta_d = 0.1$ in all three cases.

4 | CONCLUSIONS AND FUTURE WORK

In this text we derive the exact solution of the Younan-Veletsos problem in terms of elementary functions in the horizontal wavenunber space. By evaluating the solution numerically, it has been shown that there exist resonance phenomena that current simplified models do not capture, as the latter presuppose that the natural frequencies of the displacement field close to the wall resemble those of the displacement at the far-field. It has been also proven that this new resonance can lead to large forces that were previously unaccounted for in simplified models, in particular when $\nu \approx 7/16$. Comparing the exact solution to the state-of-the-art model [17] also yields as conclusion the later being safe as long as $\nu \leq 0.15$.

To formally close the problem, the inverse Fourier transform involving the coefficients in eq. (15) should be computed to obtain the exact displacement field in every point of the domain.

This exact solution can potentially be generalized to the case of *rough* wall (the soil being bonded to the wall), by mildly adapting the boundary conditions at the wall, and applying the same procedure outlined in this text; this particular case possess great interest as removing the capacity of the soil bordering the wall to deform vertically should make the second set of natural frequencies vanish. An intermediate case between the two in which the wall is neither smooth nor rough –but is governed by a certain friction law– may be also amenable utilizing a slightly different approach. Another interesting extension is the *flexible* wall case, what would provide new insight on the relation between wall stiffness and seismic earth pressures so as to confirm the insight obtained by Veletsos and

Younan through simplified models and simulations [16].

acknowledgements

The first author would like to thank Dr. C. A. Davis (LADWP) for stimulating discussions on this and other similar problems, and Prof. M. Ortiz (Caltech) for providing the impetus to face down the math.

supplementaty material

A Mathematica notebook titled *Exact Solution YV Problem.nb*, containing derivations and evaluation of the functions leading to the plots that are displayed in this text, can be found in the first author's GitHub (`github.com/jgarciasuarez`, repository name: `thesis_exactYV`).

references

[1] Lubliner J. Plasticity theory. Courier Corporation; 2008.

[2] Love AEH. A treatise on the mathematical theory of elasticity. Cambridge university press; 2013.

[3] Coulomb CA. Essai sur une application des regles de maximis et minimis a quelques problemes de statique relatifs a l'architecture (essay on maximums and minimums of rules to some static problems relating to architecture) 1973;.

[4] Building Seismic Safety Council B, NEHRP Recommended Seismic Provisions for New Buildings and Other Structures (FEMA P-750). National Institute of Building Sciences Washington, DC; 2009.

[5] Okabe S. General theory on earth pressure and seismic stability of retaining wall and dam. J of the Japan Society of Civil Engrg 1924;10(6):1277–1323.

[6] Seed H. Design of earth retaining structures for dynamic loads. In: ASCE Specialty Conf.-Lateral Stress in the Ground and Design of Earth Retaining Structures, 1970; 1970. .

[7] Steedman R, Zeng X. The influence of phase on the calculation of pseudo-static earth pressure on a retaining wall. Geotechnique 1990;40(1):103–112.

[8] Mylonakis G, Kloukinas P, Papantonopoulos C. An alternative to the Mononobe–Okabe equations for seismic earth pressures. Soil Dynamics and Earthquake Engineering 2007;27(10):957–969.

[9] Candia G, Mikola RG, Sitar N. Seismic response of retaining walls with cohesive backfill: Centrifuge model studies. Soil Dynamics and Earthquake Engineering 2016;90:411–419.

[10] Wood JH. Earthquake-induced soil pressures on structures 1973;.

[11] Matsuo H, Ohara S. Lateral earth pressure and stability of quay walls during earthquakes. In: Proceedings of the Second World Conference on Earthquake Engineering, vol. 1 Science Council of Japan Tokyo-Kyoto, Japan; 1960. p. 165–181.

[12] Verruijt A. Soil dynamics. Technische Universiteit, Faculteit Civiele Techniek; 1996.

[13] Veletsos A, Younan A. Dynamic soil pressures on rigid vertical walls. Earthquake engineering & structural dynamics 1994;23(3):275–301.

[14] Veletsos AS, Younan AH. Dynamic modeling and response of soil-wall systems. Journal of Geotechnical Engineering 1994;120(12):2155–2179.

[15] Scott R. Earthquake-induced pressures on retaining walls. In: Proceedings of the 5th World Conference on Earthquake Engineering, vol. 2; 1973. p. 1611–1620.

[16] Younan A, Veletsos AS. Dynamic response of flexible retaining walls. Earthquake engineering & structural dynamics 2000;29(12):1815–1844.

[17] Kloukinas P, Langousis M, Mylonakis G. Simple Wave Solution for Seismic Earth Pressures on Non-Yielding Walls 2012 03;138:1514–1519.

[18] Brandenberg SJ, Mylonakis G, Stewart JP. Kinematic framework for evaluating seismic earth pressures on retaining walls. Journal of Geotechnical and Geoenvironmental Engineering 2015;141(7):04015031.

[19] Keykhosropour L, Lemnitzer A. Experimental studies of seismic soil pressures on vertical flexible, underground structures and analytical comparisons. Soil Dynamics and Earthquake Engineering 2019;118:166–178.

[20] Miklowitz J. The theory of elastic waves and waveguides, vol. 22. Elsevier; 2012.

[21] Weinberger HF. A first course in partial differential equations: with complex variables and transform methods. Courier Corporation; 2012.

[22] Lang S. Complex analysis, vol. 103. Springer Science & Business Media; 2013.

[23] Wolfram S. The mathematica book, vol. 4. Cambridge University Press Cambridge; 2000.

[24] Garcia-Suarez J. Application of path-independent integrals to soil-structure interaction. PhD thesis, California Institute of Technology; 2020.

[25] Simulia DS. Abaqus analysis user's manual. Dassault Systemes, Pawtucket, USA 2010;.

[26] Esmaeilzadeh Seylabi E. Reduced order modeling of soil structure interaction problems. PhD thesis, UCLA; 2016.

[27] Durante MG, Brandenberg SJ, Stewart JP, Mylonakis G. In: Winkler Stiffness Intensity for Flexible Walls Retaining Inhomogeneous Soil; 2018. .

[28] Ostadan F. Seismic soil pressure for building walls: An updated approach. Soil Dynamics and Earthquake Engineering 2005;25(7-10):785–793.